ISSN 1995-0780, Nanotechnologies in Russia, 2010, Vol. 5, Nos. 11–12, pp. 837–843. © Pleiades Publishing, Ltd., 2010.
Original Russian Text © V.G. Zavodinsky, 2010, published in Rossiiskie nanotekhnologii, 2010, Vol. 5, Nos. 11–12.

ARTICLES

Tungsten Carbide on the Subnanoscale Level: Atomic Structure, Electronic States, and Mechanical Properties

V. G. Zavodinsky

Institute of Material Science, Khabarovsk Scientific Center, Far East Division, Russian Academy of Sciences, ul. Tikhookeanskaya 153, Khabarovsk, 680042 Russia
e-mail: vzavod@mail.ru

Received March 12, 2010

Abstract—Density functional theory and pseudopotential methods are used to study the atomic structure, electronic states, and mechanical properties of WC nanoparticles 1 nm in size and smaller. It is found that the smallest particles (containing less than 15 atomic pairs of WC) have a cubelike NaCl-type structure. In the range of 10 to 20 pairs, WC particles with cubic and trigonal structures have approximately equal energies; however, their internal atomic structure preserves the alternation pattern of W and C atoms that is inherent in NaCl. A trigonal WC_{15} particle is used to study the tensile strength and resistance to compression. It is found that the strength of the nanoparticle is much higher than the strength of the bulk material. Tungsten and carbon vacancies decrease the strength of the particles; however, cobalt atoms penetrating into the vacancy positions can restore the strength of the nanoparticles and their resistance to compression almost to values characteristic of a defect-free case. The density of electronic states of WC nanoparticles has a form close to the density of states of the bulk cubic phase of tungsten carbide exhibiting a metallic nature with a high density near the Fermi level.

DOI: 10.1134/S1995078010110133

INTRODUCTION

Hard alloys based on tungsten carbide (WC crystallites inside the Co matrix) are widely used as a material for cutting tools. Recent studies show that the performance capabilities of hard alloys are significantly improved due to a decrease in the crystallite size down to 300–500 nm [1–4]. However, the nature of this change is vague. Moreover, it is not clear how the properties of hard alloys will change after a further decrease in WC crystallites. In addition, there is no information on the atomic and electronic structure of WC nanoparticles and their mechanical properties. It is shown [5, 6] that nanoparticles 300–500 nm in size have a triangular exterior shape; however, their internal atomic structure is unknown. Cobalt is a separate issue. The studies of the WC/Co interface using high-resolution electron microscopy show [7] that cobalt can penetrate into WC crystallites. The following question arises: is its role limited only to a cementing function or does cobalt actively affect the mechanical properties of tungsten carbide?

In this work we carry out a quantum-mechanical (from first principles) simulation of tungsten carbide nanoparticles and study their electronic structure and mechanical properties. Unfortunately, a first-principle simulation of WC nanoparticles with sizes that are of direct interest for the technology (50–100 nm) is technically impossible at this time; therefore, we were restricted to studying particles of WC_N (N = 2–40) with a size of up to 1 nm. However, from general physical considerations we can expect that the results of this work will be useful for understanding and predicting the properties of larger WC nanoparticles.

COMPUTING TECHNIQUE AND DETAILS

The total energy, electronic structure, and mechanical properties of WC nanoparticles were cal-

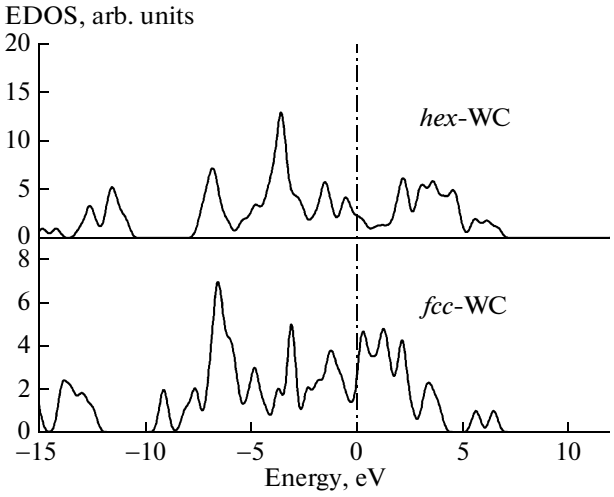

Fig. 1. Calculated EDOS for bulk hexagonal (*hex*-WC) and cubic (*fcc*-WC) tungsten carbide. The vertical dotted line denotes the Fermi level.

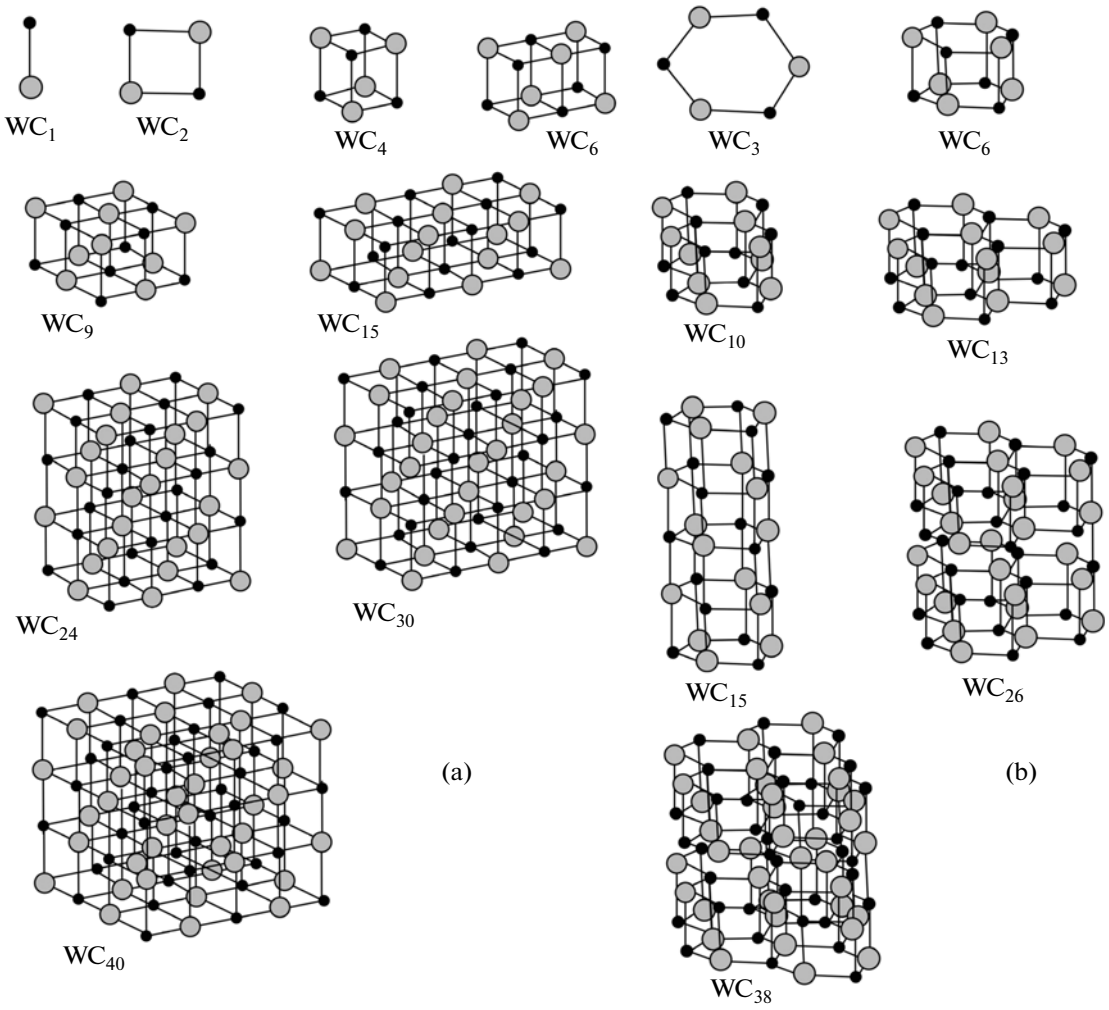

Fig. 2. Atomic arrangements of WC nanoparticles with (a) cubic and (b) trigonal structures. The small black circles denote carbon atoms; the large gray circles stand for tungsten atoms.

culated using the FHI96spin software package, which is a modification of the FHI96md package [8], which has been used previously for many systems, including nanoparticles of transition metals and their compounds [9–12]. This package is based on the spin-polarized version of the density functional theory [13, 14], the pseudopotential method [15], and the use of a set of plane waves. In this work we used the pseudopotentials of carbon and cobalt constructed using the FHI98PP package [16] according to the Troullier–Martins scheme [17]; the Hamann scheme was used for tungsten [18]. All these potentials are separable, transferable, and norm- conserving. They are checked for the absence of so-called "ghost" states and used for the test determination of equilibrium lattice parameters and bulk modulus of elasticity. The parameters of the pseudopotential are listed in Table 1.

In all cases we used the generalized gradient approximation [19] and optimized the atomic geometry to take into account the exchange–correlation

Table 1. Critical radii for the *s*, *p*, and *d* components (r_s, r_p, r_d) and type of the local part (l_{loc}) of pseudopotentials

Element	r_s, Å	r_p, Å	r_d, Å	l_{loc}
W	1.57	1.78	0.88	*s*
C	1.50	1.50	1.50	*d*
Co	2.18	2.92	2.18	*s*

Table 2. Average lengths of the W–C bonds ($d(W–C)_{av}$) in cubic and trigonal WC particles

	WC_6		WC_{15}		WC_{24}		WC_{36}	
	Cub.	Trigon.	Cub.	Trigon.	Cub.	Trigon.	Cub.	Trigon.
$d(W–C)_{av}$, Å	2.07	1.98	2.11	2.04	2.12	2.04	2.13	2.04

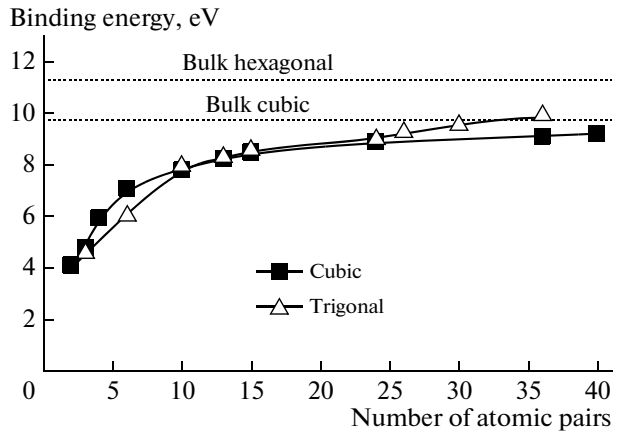

Fig. 3. Dependence that the binding energy (per one atomic pair of WC) has on the structure and size of the WC nanoparticle.

interaction. The equilibrium lattice parameters and elastic moduli were calculated using the Murnagham equation of state [20].

Since the FHI96spin package operates with periodic wave functions, we used a cubic supercell with a size of 30 au (1 au is equal to 0.0529 nm) to study the nanoparticles; this was large enough to study nanoparticles with the number of WC pairs reaching 40 as single noninteracting particles. In most cases (except for bulk calculations) we used only one point of the Brillouin zone, namely, the Gamma point (0, 0, 0). For bulk calculations we used the Monkhorst–Pack schemes ($3 \times 3 \times 3$ and $5 \times 5 \times 5$) [21] with the number of k-points reaching 27. The cutoff energy for the set of plane waves was 40 Ry. The self-consistency in the energy occurred with an accuracy of 0.005 eV.

BULK WC

The structure of bulk tungsten carbide is well known. Hexagonal WC exists below 2525°C; cubic *fcc*-WC with a NaCl-type structure is stable above this temperature [22].

For *hex*-WC, we found the equilibrium lattice constant $a = 2.92$ Å, the cohesive energy $E = 9.69$ eV, and the bulk modulus $B = 388$ GPa. The experimental values are $a = 2.91$ Å, $E = 8.34$ eV, and $B = 331$ GPa [23]. The published theoretical data fall in the ranges of 2.88–2.92 Å, 379–413 GPa, and 8.14–9.72 eV, respectively [24].

For cubic *fcc*-WC, the calculated values of the lattice constant and cohesive energy are $a = 4.39$ Å and $E = 8.89$ eV. The respective published values are 4.29–4.38 Å and 7.71–9.46 eV [23].

In addition, we calculated the electron density of the states (EDOS) (Fig. 1). The EDOS curves for *hex*-WC and *fcc*-WC are extremely similar to the results shown in other theoretical works [23, 25, 26]. The main difference between *fcc*-EDOS from *hex*-EDOS lies in the different values of EDOS at the Fermi level. That is, in the hexagonal case, the Fermi level is situated near the minimum of the curve; in the cubic case, it is near the maximum.

ATOMIC STRUCTURE AND ELECTRONIC STATES OF NANOPARTICLES

There are experimental and theoretical data [5, 27–31] that show that nanocrystals of tungsten carbide are triangular rather than hexagonal. However, the atomic structure of WC nanoparticles and their electronic and other properties are not known.

We studied stoichiometric particles with the number (N) of WC pairs from 2 to 40 by comparing their binding energy per one WC pair. First of all, we found that NaCl-type bonds are preferential for all studied particles. Hexagonal particles with the arrangement of W and C atoms similar to bulk *hex*-WC (layerwise) are unstable and tend to spontaneously rearrange themselves into particles with a trigonal symmetry and a NaCl-type ordering. Trigonal particles compete with

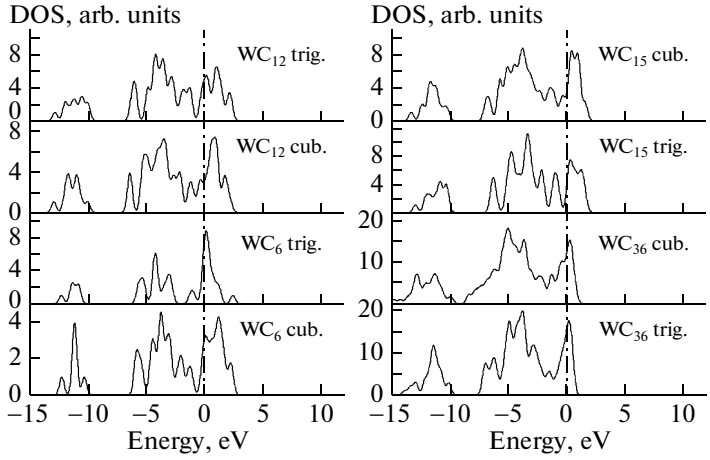

Fig. 4. DOS for cubic and trigonal WC nanoparticles. The vertical dotted lines denote the Fermi level.

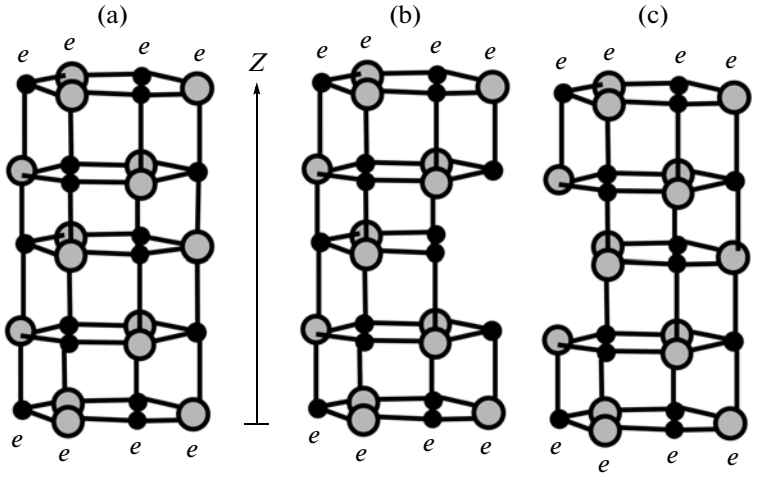

Fig. 5. Atomic arrangements used to study the tensile strength of a trigonal WC_{15} particle: (a) ideal particle, (b) particle with a W vacancy, and (C) particle with a C vacancy. The vertical arrow Z indicates the direction of elongation; the symbols e stand for outermost atoms.

cubic particles: the latter are advantageous for $N < 15$ and the former are advantageous for $N > 15$. The atomic arrangements of typical particles with cubic and trigonal symmetries are shown in Figs. 2A and 2B; the dependence that the binding energy has on the structure and size of the particles is depicted in Fig. 3.

Despite the fact that the binding of W and C atoms in nanoparticles has the same type of NaCl as in bulk *fcc*-WC, the lengths of these bonds differ from crystalline ones. For example, in a relaxed trigonal WC_{15} particle, the W–C distances range from 1.98 to 2.20 Å, and in a cubic WC_{24} particle they are 1.98 Å in the corners of the particles and increase up to 2.40 Å while approaching the center. In general, the average W–C distances ($d(W–C)_{av}$) in trigonal particles are smaller than in cubic (see Table 2). In addition, the average W–C distances in trigonal particles rapidly converge to 2.04 Å, while in cubic particles they tend to increase up to a bulk value of 2.20 Å. This is possibly the main reason that trigonal particles become more advantageous with an increase in particle size.

The electronic structure of WC nanoparticles is shown in Fig. 4. All the plotted densities of states (DOS) are similar to the DOS of bulk *fcc*-WC, which is shown above in Fig. 1 and whose Fermi level is situated not far from the local maximum of DOS. We can assume that the nature of this similarity lies in the similarity between the type of bonds of W and C atoms in nanoparticles (both trigonal and cubic) and the type of bonds in bulk *fcc*-WC. In all these cases, this is the type of NaCl.

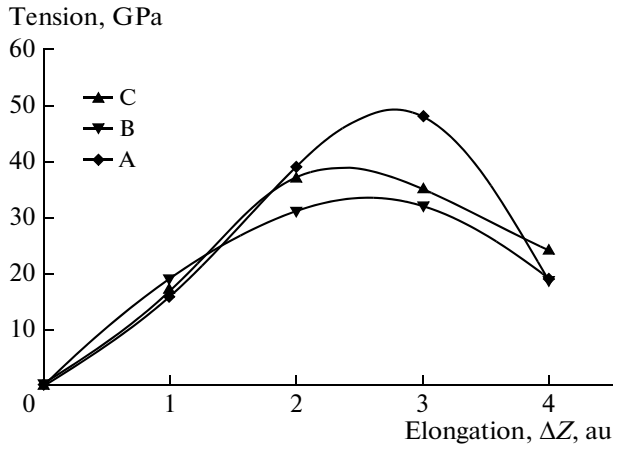

Fig. 6. Dependence that tension has on the elongation of trigonal WC_{15} particles: (A) ideal particle, (B) particle with a W vacancy, and (C) particle with a C vacancy.

TENSILE STRENGTH AND RESISTANCE TO COMPRESSION: EFFECT OF COBALT

Strength is one of the most important mechanical properties of tungsten carbide as a material for cutting tools. Since trigonal particles are more stable in real sizes, we confined ourselves to this particular case for studying strength. Namely, a WC_{15} particle was selected for the study.

To determine the ultimate tensile strength, we elongated the WC_{15} particle stepwise along the Z direction; each time, we fixed the coordinates of the outermost atoms and let all the other atoms relax (Fig. 5). The value of tension T was calculated through the derivative of the total energy E as a function of z:

$$T = \frac{dE}{dz}\frac{1}{S},$$

where S is the cross-sectional area of the particle in the XY plane.

The dependence of tension as a function of elongation ΔZ for an ideal particle is depicted in Fig. 6 (curve A).

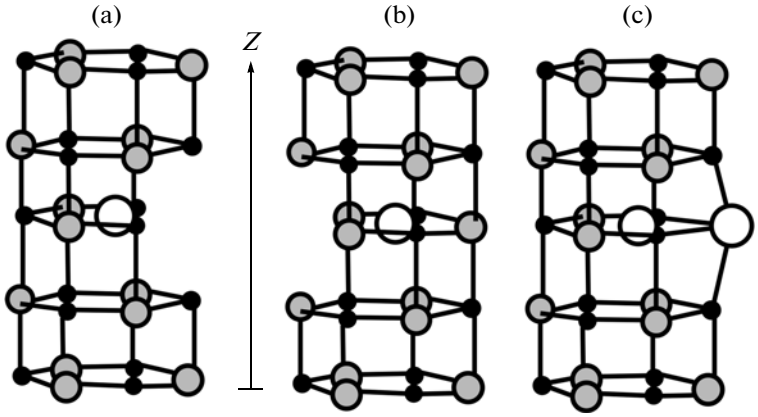

Fig. 7. Atomic arrangements used to study the tensile strength of a trigonal WC_{15} particle doped with cobalt: the white circles stand for cobalt atoms: (a) particle with a W vacancy and one atom of cobalt inside, (b) particle with a C vacancy and one atom of cobalt inside, and (c) particle with a W vacancy and two atoms of cobalt (one inside and the other outside).

The maximum of this dependence corresponds to 48 GPa, which is appreciably higher than the known values of bulk tungsten carbide (0.3–0.4 GPa) and hard alloys on its basis (0.5–2.0 GPa). The same figure shows the results of similar calculations for particles with vacancies: with a W vacancy (curve *B*) and with a C vacancy (curve *C*). We can see that the vacancies reduce the tensile strength; however, this effect is not too significant: the coefficient of reduction of the tensile strength does not exceed 0.7–0.8. That is, defective nanoparticles preserve their strength fairly well.

In WC/Co hard alloys, particles of tungsten carbide are surrounded by cobalt atoms. If the WC particles have some surface defects (vacancies in our case), the cobalt atoms can interact with them and even penetrate into the surface layers of the particle, as was noted in experimental studies [7]. Some examples of this situation are illustrated in Fig. 7, where, in cases (A) and (B), the cobalt atoms penetrate into the WC particle through W and C vacancies, respectively, while in case (C) one atom of cobalt penetrates into the particle and the other Co atom fills the vacancy. In addition, in case (A), the Co atom penetrates into the particle without barriers and, in case (B), the height of the energy barrier is fairly small (about 0.5 eV). Figure 8 shows the dependence that tension has on the elongation of the WC_{15} particle for these three cases.

It is clear from a comparison of Figs. 8 and 6 that cobalt atoms can increase the tensile strength of defective WC particles up to 90% of the value characteristic of a defect-free state. In other words, cobalt can heal some surface defects of WC particles and improve their properties.

Since the case at hand is hard materials, it is only natural to place a special emphasis on their hardness. However, hardness is a technical characteristic and has no exact physical equivalent. It is impossible to directly compare the hardness of a bulk material and nanoparticles. Moreover, in this work, we were interested in the effect that defects have on the hardness of nanoparticles rather than on hardness as such. Therefore, we studied the resistance of the WC_{15} nanoparticle to compression and paid particular attention to the effect that cobalt atoms have on this process.

The scheme of the study is clear from Fig. 9. A trigonal WC_{15} particle ((*A*) ideal, (*B*) having a W vacancy, and (*C*) having a W vacancy and doped with two atoms of cobalt) was compressed in the *X* direction perpendicular to the *YZ* plane. The atomic arrangements for the particles (ideal, having a vacancy, and doped) were taken the same as in the study of tensile strength. The outermost atoms (marked with the symbol *e*) were shifted before each step of calculations and fixed during this step, whereas the other atoms were free to

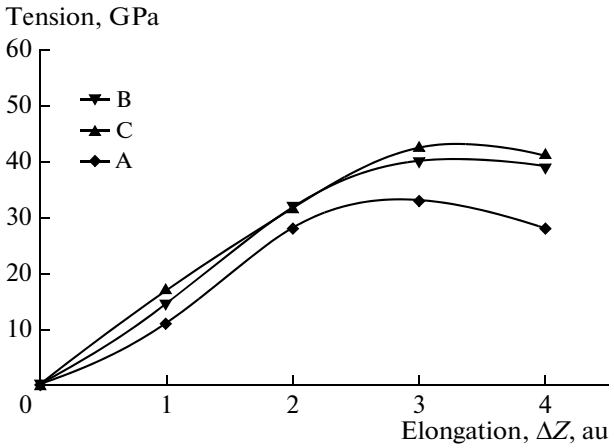

Fig. 8. Dependence that tension has on the elongation of a trigonal WC_{15} particle doped with cobalt: (A) particle with a W vacancy and one atom of cobalt inside, (B) particle with a C vacancy and one atom of cobalt inside, and (C) particle with a W vacancy and two atoms of cobalt (one inside and the other outside).

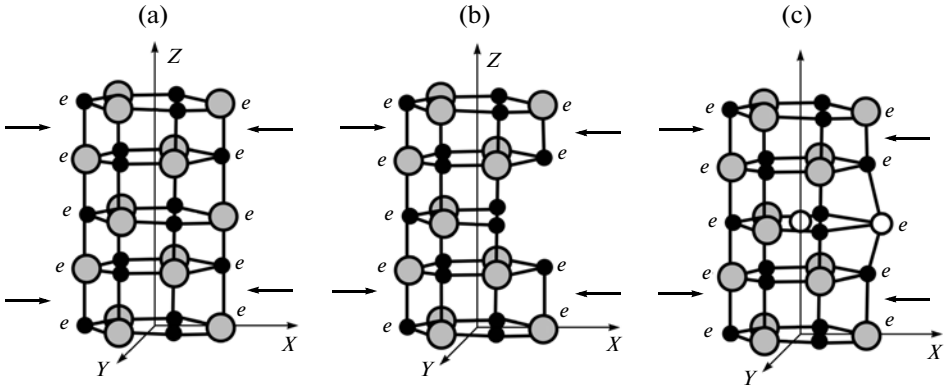

Fig. 9. Scheme of the study of the response of the WC_{15} particle to compression: (a) ideal case, (b) W vacancy, and (c) W vacancy and two atoms of cobalt.

relax. The value of pressure acting on the particle was calculated through the derivative of the total energy E as a function of x:

$$P = \frac{dE}{dx}\frac{1}{S_{Y,Z}},$$

where S is the sectional area of the particle in the YZ plane.

The dependence that pressure P has on compression Δx for all the studied cases is shown in Fig. 10. It is easy to see that the vacancy defect makes the nanoparticle less hard; however, a nanoparticle with a vacancy healed by cobalt can resist compression approximately half as much as an ideal particle. In other words, we can say that cobalt in a hard WC/Co alloy not only plays the role of a cementing link but also can penetrate into the surface layers of WC crystallites and increase their hardness.

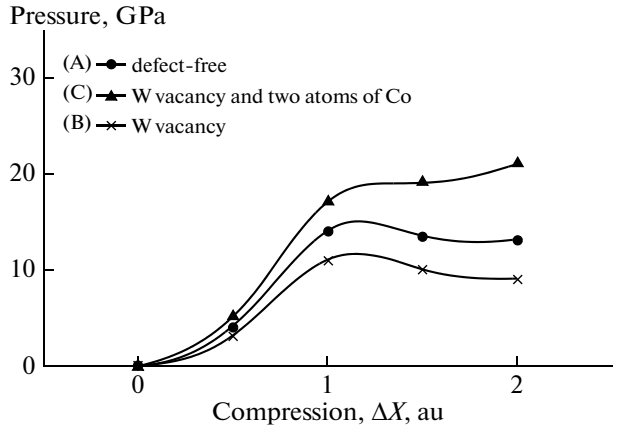

Fig. 10. Dependence that pressure has on the compression of the trigonal WC_{15} particle: (A) ideal case, (B) W vacancy, and (C) W vacancy and two atoms of cobalt.

CONCLUSIONS

Quantum-mechanical calculations confirm that WC nanoparticles larger than 1 nm exhibit a trigonal symmetry. The tensile strength for the nanoparticles is higher by a factor of 10–15 than for the bulk material. Cobalt atoms can heal some surface defects of WC particles and improve their mechanical properties.

ACKNOWLEDGMENTS

This work was supported by the Presidium of the Far East Division of the Russian Academy of Sciences and the Russian Foundation for Basic Research.

REFERENCES

1. W. D. Schubert, A. Bock, and B. Lux, "General Aspects and Limits of Conventional Ultrafine WC Powder Manufacture and Hard-Metal Production," Int. J. Refract. Met. Hard Mater. **13**, 281–286 (1995).
2. K. Jia, T. E. Fischer, and B. Gallois, "Microstructure, Hardness, and Toughness of Nanostructure and Conventional WC–Co Composites," Nanostruct. Mater. **10**, 875–891 (1998).
3. B. K. Kim, G. H. Ha, D. W. Lee, G. G. Lee, and I. S. Ahn, "Chemical Processing of Nanostructured Cemented Carbide," Adv. Perform. Mater. **5**, 341–352 (1998).
4. J. A. M. Ferreira, M. A. Pina Amaral, F. V. Antunes, and J. D. M. Costa, "A Study on the Mechanical Behavior of WC/Co Hard Metals," Int. J. Refract. Met. Hard Mater. **27**, 1–8 (2009).
5. M. Christensen, G. Wahnström, C. Alibert, and S. Lay, "Quantitative Analysis of WC Grain Shape in Sintered WC–Co Cemented Carbides," Phys. Rev. Lett. **94**, 066 105–066 108 (2005).
6. A. Delanoe and S. Lay, "Evolution of the WC Grain Shape in WC–Co Alloys during Sintering: Effect of C Content," Int. J. Refract. Met. Hard Mater. **27**, 140–148 (2009).
7. T. Yamamoto, Y. Ikuhara, T. Watanabe, T. Sakuma, Y. Taniuchi, K. Okada, and T. Tanase, "High-Resolu-

tion Electron Microscopy Study in Cr_3C_2-Doped WC–Co," J. Mater. Sci. **36**, 3885–3890 (2001).

8. M. Beckstedte, A. Kley, J. Neugebauer, and M. Scheffler, "Density Functional Theory Calculations for Poly-Atomic Systems: Electronic Structure, Static and Elastic Properties, and Ab Initio Molecular Dynamics," Comput. Phys. Commun. **107**, 187–205 (1997).
9. J. Dabrowski, H.-J. Mussig, V. G. Zavodinsky, R. Baierle, and M. J. Caldas, "Mechanism of Dopant Segregation to SiO_2/Si(001) Interfaces," Phys. Rev. B; Condens. Matter **65**, 245 305 (2002).
10. V. G. Zavodinsky, "The Mechanism of Ionic Conductivity in Stabilized Cubic Zirconia," Phys. Solid State **46** (3), 453–457 (2004).
11. V. G. Zavodinsky and A. N. Chibisov, "Zirconia Nanoparticles and Nanostructured Systems," J. Phys.: Conf. Ser. **29**, 173–176 (2006).
12. V. G. Zavodinsky, "Quantum-Mechanical Study of Elastic Properties of Nanoparticles and Their Agglomeration Processes," Ross. Nanotekhnol. **2** (11–12), 58–62 (2008) [Nanotechnol. Russ. **2** (11–12), 691–696 (2008)].
13. H. Hohenberg and W. Kohn, "Inhomogeneous Electron Gas," Phys. Rev. Sect. B **136**, 864–871 (1964).
14. W. Kohn and J. L. Sham, "Self-Consistent Equations Including Exchange and Correlation Effects," Phys. Rev. Sect. A **140**, 1133–1138 (1965).
15. M. Cohen and V. Heine, "Pseudopotential Theory of Cohesion and Structure," in *Solid State Physics*, Ed. by H. Ehrenreich, F. Seitz, and D. Turnbull (Academic, New York, 1970), Vol. 24, p. 250.
16. M. Fuchs and M. Scheffler, "Ab Initio Pseudopotentials for Electronic Structure Calculations of Poly-Atomic Systems Using Density Functional Theory," Comput. Phys. Commun. **119**, 67–165 (1999).
17. N. Troullier and J. L. Martins, "Efficient Pseudopotentials for Plane-Wave Calculations," Phys. Rev. B: Condens. Matter **43**, 1993–2006 (1991).
18. D. R. Hamann, "General Norm-Conserving Pseudopotentials," Phys. Rev. B: Condens. Matter **40**, 2980–2991 (1989).
19. J. P. Perdew and Y. Wang, "Accurate and Simple Density Functional for the Electronic Exchange Energy," Phys. Rev. B: Condens. Matter **33**, 8800–8802 (1986).
20. F. D. Murnagham, "The Compressibility of Media under Extreme Pressures," Proc. Natl. Acad. Sci. USA **30**, 244–247 (1944).
21. H. J. Monkhorst and J. D. Pack, "Special Points for Brillouin-Zone Integrations," Phys. Rev. B: Solid State **13**, 5188–5192 (1976).
22. Chemical encyclopedia/tungsten carbide http://www.xumuk.ru/encyklopedia/813.html.
23. D. L. Price and B. P. Cooper, "Total Energies and Bonding for Crystallographic Structures in Titanium–Carbon and Tungsten–Carbon Systems," Phys. Rev. B: Condens. Matter **39**, 4945–4977 (1989).
24. M. Christensen and G. Wahnstr[sign: umlaut]om, "Co-Phase Penetration of WC($10\bar{1}\bar{0}$)/WC($10\bar{1}\bar{0}$) Grain Boundaries from First Principles," Phys. Rev. B: Condens. Matter **67** (11), article 115 415 (11 pages) (2003).
25. L. F. Mattheiss and D. R. Hamann, "Bulk and Surface Electronic Structure of Hexagonal WC," Phys. Rev. B: Condens. Matter **30**, 1731–1738 (1984).
26. A. Y. Liu, R. M. Wentzcovitch, and M. L. Cohen, "Structural and Electronic Properties of WC," Phys. Rev. B: Condens. Matter **38**, 9483–9489 (1989).
27. F. R. N. Nabarro, L. S. Bartolucci, and U. V. Waghmare, "Slip in Tungsten Monocarbide: I. Some Experimental Observations," Mater. Sci. Eng., A **483–484**, 139–142 (2008).
28. F. R. N. Nabarro, L. S. Bartolucci, and U. V. Waghmare, "Slip in Tungsten Monocarbide: II. A First-Principles Study," Mater. Sci. Eng., A **483–484**, 9–12 (2008).
29. C.-S. Kim and G. S. Rohrer, "Geometric and Crystallographic Characterization of WC Surfaces and Grain Boundaries in WC–Co Composites," Interface Sci. **12** (1), 19–27 (2004).
30. A. V. Shatov, S. A. Firstov, and I. V. Shatova, "The Shape of WC Crystals in Cemented Carbides," Mater. Sci. Eng., A **242**, 7–14 (1998).
31. S. Kim, S.-H. Han, J.-K. Park, and H.-E. Kim, "Variation of WC Grain Shape with Carbon Content in the WC–Co Alloys during Liquid-Phase Sintering," Scr. Mater. **48** (5), 635–639 (2003).